questions. The first is whether there are multiple components to the mesodermal inductive signal. Slack *et al.* (*4*) found that bovine FGF induces predominantly ventrolateral mesodermal tissues such as blood, mesenchyme, and muscle, but only very rarely induces notochord, the most characteristic dorsal mesodermal structure. In contrast, Smith (*3*) found that the *Xenopus* MIF commonly induces both muscle and notochord. We observed induction of muscle and, at lower frequency, notochord by middle T. Whether these differences simply reflect the relative strengths of the inducing signals generated by FGF, MIF, and middle T or the generation of a distinct "dorsalizing" signal remains to be determined.

A second question is whether activation of any of a number of distinct mitogenic and oncogenic signaling pathways is sufficient to induce mesoderm. Although Slack *et al.* (*4*) found that FGF and embryonal carcinoma-derived growth factor (ECDGF) were the only peptide mitogen among many tested to induce mesoderm, it is not known whether this specificity is determined by receptor expression or the activation of an FGF-specific intracellular signaling pathway. Although there is evidence that the fibroblast mitogen platelet-derived growth factor (PDGF) may activate similar signaling pathways to those activated by middle T (*21, 24*), there is no direct evidence that FGF shares these same signaling pathways. FGF does, however, appear to elevate cellular diacylglycerol (*25*) and to increase cellular tyrosine phosphorylation (*26*), suggesting that FGF- and middle T–activated signal transduction pathways may overlap. Introduction of other oncogenes (for example, p21ras) or growth factor receptors (for example, PDGF receptor) may clarify whether the mesodermal differentiative program is activated by a single, specific intracellular signal or by any of a number of mitogen-stimulated mediators.

The third question is whether the intracellular signaling pathway (or pathways) is actually activated during the natural inductive process. The observation that middle T can activate mesodermal differentiation does not in itself demonstrate that natural mesodermal induction is mediated by any of the known middle T targets (for example, $pp60^{c\text{-}src}$, $pp62^{c\text{-}yes}$, and PI(3) kinase). Furthermore, it does not address the question of how many different types of endogenous or artificial signals may be capable of inducing mesoderm. It does, however, indicate cellular regulatory proteins that may be investigated as potential mediators of natural inductive signals. Further work to clarify the number and specificity of possible intracellular messengers of mesodermal induction is necessary; the microinjection of mRNAs encoding putative regulators should prove useful in addressing these points.

REFERENCES AND NOTES

1. P. Nieuwkoop, *Wilhelm Roux Arch. Entwicklungsmech. Org.* **162**, 341 (1969).
2. J. Gurdon, *Development* **99**, 285 (1987).
3. J. C. Smith, *ibid.*, p. 3.
4. J. M. W. Slack *et al.*, *Nature* **326**, 197 (1987).
5. D. Kimelman and M. Kirschner, *Cell* **51**, 869 (1987).
6. F. Rosa *et al.*, *Science* **239**, 783 (1988).
7. D. L. Weeks and D. Melton, *Cell* **51**, 861 (1987).
8. A. P. Otte *et al.*, *Nature* **334**, 618 (1988).
9. A. Hunter and J. Cooper, *Annu. Rev. Biochem.* **54**, 897 (1985).
10. M. Whitman and L. Cantley, *Biochim. Biophys. Acta* **948**, 327 (1988); E. Rozengurt, *Science* **234**, 161 (1986); R. A. Weinberg, *ibid.* **230**, 770 (1985).
11. S. Courtneidge and A. E. Smith, *Nature* **303**, 435 (1983).
12. J. B. Bolen *et al.*, *Cell* **38**, 767 (1984).
13. S. Kornbluth *et al.*, *Nature* **325**, 171 (1986); D. R. Kaplan *et al.*, *Biochim. Biophys. Acta* **948**, 345 (1988).
14. M. Whitman *et al.*, *Nature* **315**, 239 (1985).
15. M. Whitman *et al.*, *ibid.* **332**, 644 (1988).
16. K. Symes and J. Smith, *Development* **101**, 339 (1987).
17. C. R. Kintner and J. P. Brockes, *Nature* **308**, 67 (1984).
18. H. R. Woodland and E. A. Jones, *Development* **101**, 925 (1987).
19. D. A. Melton, unpublished data.
20. M. Whitman and D. A. Melton, unpublished data.
21. D. R. Kaplan *et al.*, *Cell* **50**, 1021 (1987).
22. H. Piwnica-Worms *et al.*, *ibid.* **49**, 75 (1987).
23. M. Noda *et al.*, *Nature* **318**, 73 (1985); S. Alema, P. Casalbore, E. Agostini, F. Tato, *ibid.* **316**, 557 (1985).
24. V. Cherington *et al.*, *Proc. Natl. Acad. Sci. U.S.A.* **83**, 4307 (1986).
25. K. Kaibuchi *et al.*, *J. Biol. Chem.* **259**, 3077 (1986).
26. E. B. Pasquale, P. A. Maher, S. J. Singer, *J. Cell Physiol.* **137**, 146 (1988).

27. We thank T. Roberts, H. Piwnica-Worms, and B. Morgan for src and middle T cDNAs and D. Pallas for antibody. M.W. was supported by a fellowship from the Jane Coffin Childs Memorial Fund for Medical Research; D.M. was supported by a grant from the NIH.

23 December 1988; accepted 21 March 1989

Global Sea Level Rise and the Greenhouse Effect: Might They Be Connected?

W. R. PELTIER AND A. M. TUSHINGHAM

Secular sea level trends extracted from tide gauge records of appropriately long duration demonstrate that global sea level may be rising at a rate in excess of 1 millimeter per year. However, because global coverage of the oceans by the tide gauge network is highly nonuniform and the tide gauge data reveal considerable spatial variability, there has been a well-founded reluctance to interpret the observed secular sea level rise as representing a signal of global scale that might be related to the greenhouse effect. When the tide gauge data are filtered so as to remove the contribution of ongoing glacial isostatic adjustment to the local sea level trend at each location, then the individual tide gauge records reveal sharply reduced geographic scatter and suggest that there is a globally coherent signal of strength 2.4 ± 0.90 millimeters per year that is active in the system. This signal could constitute an indication of global climate warming.

DURING THE PAST CENTURY, SEA level, as recorded on tide gauges situated at stations around the world, has apparently risen by 10 to 20 cm, no more than 25% of which may apparently be attributed to the steric effect of thermal expansion of the oceans (*1–3*). The dominant cause of rising sea levels must therefore be the increase of the mass of water in the global oceans, most probably due to melting of land-based ice sheets and glaciers (*4*). Because general circulation model simulations have shown that the climatic warming expected from increasing atmospheric loads of CO_2 and other greenhouse gases is strongly focused in polar latitudes [for example (*5*)], observations of rising sea level have been construed as a first indication of this climatic change (*1, 2*).

A serious impediment to acceptance of this interpretation has been that the observed rates of sea level rise exhibit such large geographic variability (the standard deviation is as large as the mean) as to seriously question the hypothesis that they reveal any globally coherent signal. The problem is especially acute because the coverage of the southern oceans with gauges of sufficient seniority is poor. In this report we demonstrate that when the tide gauge data are corrected for contamination due to the ongoing influence of glacial isostatic adjustment, the global pattern thereby revealed does have high spatial coherence.

The process of glacial isostatic adjustment continues to substantially influence the record of relative sea level (RSL) change, even though the last major deglaciation event was complete more than 6000 years ago, because

Department of Physics, University of Toronto, Toronto, Ontario, Canada M5S 1A7.

the high viscosity of the planetary mantle results in a slow restoration of gravitational equilibrium subsequent to deglaciation [for example (*6*)]. Present-day rates of RSL rise due to this cause are a strong function of geographic location; rates as low as −1.2 cm per year occur at sites that were once ice covered and rates as high as 2 mm per year occur at sites immediately peripheral to the ice-loaded regions (*6*). This influence must therefore be accurately filtered from the tide gauge data in order to use them as a basis for inference of the component of RSL rise that could be associated with global climatic change.

To accurately remove this contamination from the records, we have used a global model of the secular sea level change due to this cause that was originally developed (*7*) for inference of mantle visoelastic structure from radiocarbon-dated records of postglacial RSL change. Such records are now available from many locations (Fig. 1). Two different functionals of the geophysical model must be specified for prediction of such RSL histories; a space-time history of deglaciation and a radial viscoelastic structure for the interior of the planet. The radiocarbon records of RSL change and other data related to the isostatic adjustment process, namely anomalies in the earth's rotation and properties of its gravitational field, are fit to iteratively determine these required functionals (*8*).

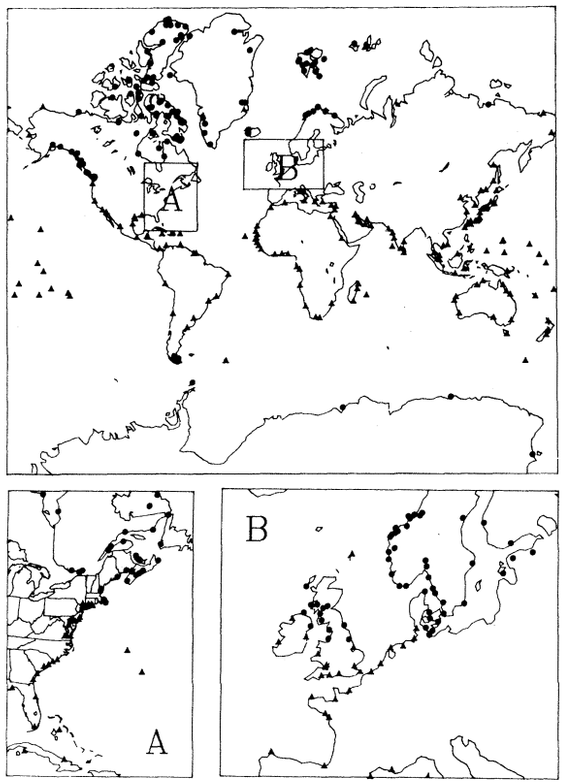

Fig. 1. Locations from which radiocarbon data are available that may be employed to define a local history of RSL change for some interval of time since the onset of the last deglaciation event of the present ice age. Locations marked with solid circles were ice-covered at glacial maximum whereas those shown as triangles were not. See (*9*) for data listings.

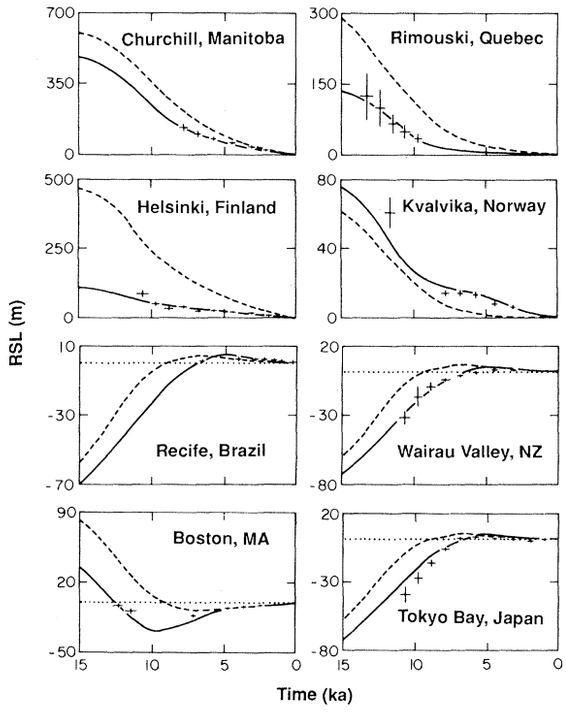

Fig. 2. Examples of comparisons between the RSL histories predicted with the geophysical model (solid and dashed curves) and radiocarbon-dated shorelines (solid crosses indicate errors) at ice-covered and ice-free sites. The geophysical predictions are from a new high-resolution model that is used for all the calculations (solid curves) and an earlier low-resolution version of the same model (*8*). The viscoelastic earth structure employed in the model has a 1066B elastic component (*8*), a lithospheric thickness of 120 km, an upper mantle viscosity of 10^{21} Pa s and a lower mantle viscosity of 2×10^{21} Pa s; ka, thousand years ago.

Comparisons of the theoretical RSL predictions with observations based on the radiocarbon data demonstrate that the geophysical model is accurate both at sites that were ice-covered and those that were not (Fig. 2). To achieve these fits, we have employed a model with considerably higher spatial resolution than previously, with respect to the representations of both the deglaciation history and ocean loading. In that the model provides close fits to observed postglacial RSL histories, it may then be used to predict the global pattern of the present-day rate of RSL change that should obtain at every point on the earth's surface. We have computed this rate of change on a fine grid of points on the surface and interpolated to generate a continuous field.

In general, the model results for this field (Fig. 3) show that high rates of sea level fall (>1 cm per year) are characteristic of regions that were once ice-covered, whereas moderately high rates of RSL rise (>2 mm per year) are predicted to occur in the immediately peripheral region. The model also predicts that the major ocean basins have a moderately high (~0.4 mm per year) rate of present-day RSL fall associated with their interiors, and that a low rate of rise obtains in a semicontinuous "halo" surrounding the major continental blocks.

To isolate any component of present-day global sea level rise (fall) that may be superimposed on this geophysical signal [as suggested by the preliminary analysis in (*10*)], we analyzed 500 tide gauge records of duration in excess of 10 years (*11*) whose locations are widely distributed [the distribution is similar to that of the radiocarbon data (Fig. 1) except that northern Canada is nearly devoid of gauges because of winter sea-ice conditions]. From this basic data set a number of records were removed ab initio, because they were either from sites that were obviously tectonically active (for example, Japan and Alaska), subsiding because of

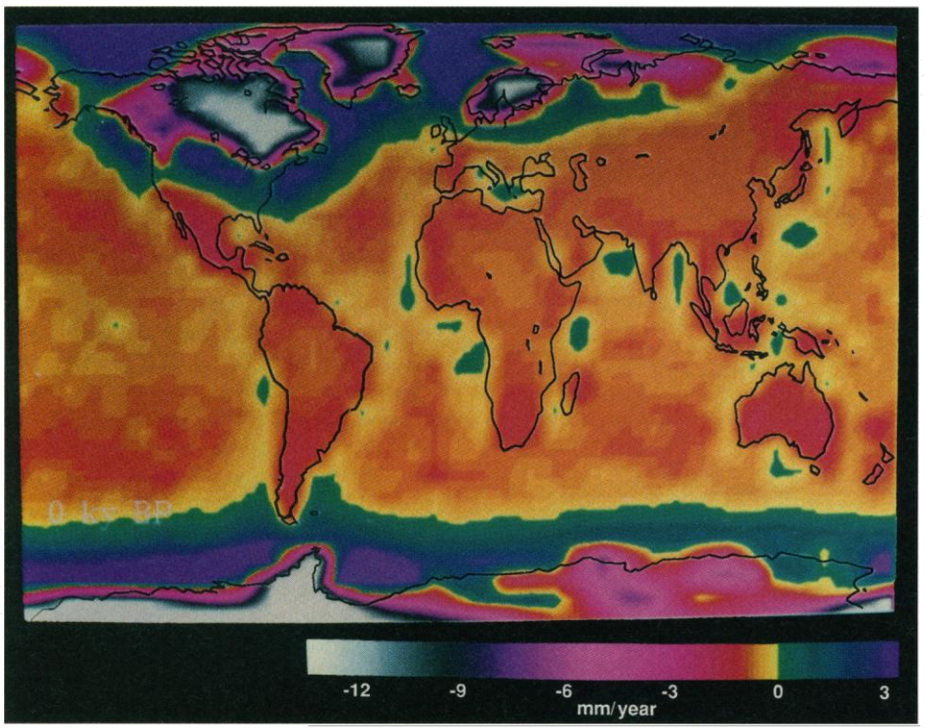

Fig. 3. The present-day rate of RSL rise (fall) that should be recorded on a modern tide gauge if the effect of glacial isostatic adjustment were the only contribution to present-day RSL change. The rates of RSL rise (fall) are in millimeters per year. Values shown over the continents represent the time rates of separation between the geoid and the surface of the solid earth.

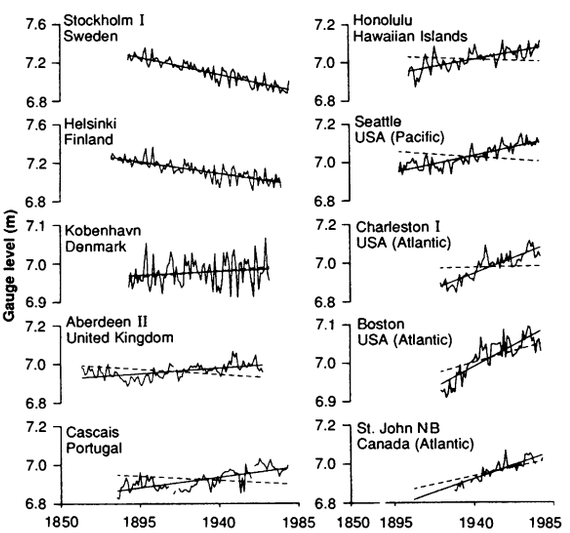

Fig. 4. Tide gauge data from representative sites upon which are superimposed the linear least squares best fit to the data (solid lines) and the predicted secular RSL trend based on the high-resoluton geophysical model (Fig. 3) (dashed lines). The geophysical signal due to glacial isostasy almost perfectly fits the data at sites that were ice-covered; NB, New Brunswick.

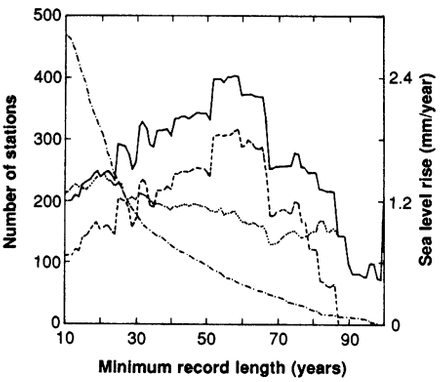

Fig. 5. Results for the global rate of RSL rise obtained from LR analysis. The dash-dotted curve depicts the decrease in the number of tide gauge stations as the miminum record length employed in the analysis increases. The three individual estimates of the globally averaged rate of RSL rise versus minimum record length are based on equal area averages of the raw (dashed curve) and reduced (solid curve) tide gauge data and a site by site average of the reduced data (dotted curve). The solid curve should provide the most accurate LR estimate of the present-day global rate of RSL rise.

sedimentary loading (for example, the Mississippi delta), or were curiously anomalous (for example, Xiamen, China, where the rate of present-day RSL rise is apparently near 13.3 mm per year). For the remaining 470 records (all represented by monthly means), we compared the secular RSL trend at each site predicted by the geophysical model with that recorded on the corresponding tide gauge record (Fig. 4). For the ten examples shown in Fig. 4, the geophysical model is seen to reconcile completely the large rates of RSL fall at sites that were once ice-covered, but at other locations there are large misfits, and the geophysically predicted rate of RSL rise is smaller than that observed on the tide gauge record at most such sites.

We have applied two different statistical estimation techniques to the reduced tide gauge data set generated by subtracting the sea level trend predicted by the isostatic adjustment model from the monthly mean tide gauge signals, namely linear regression (LR) analysis and empirical orthogonal function (EOF) analysis. Use of two methods that have different strengths provides a useful cross-check on our results. Only those records that are continuous through an identical period of time could be used in the EOF analysis, whereas all records could be employed in the LR analysis. The LR technique, however, provides no direct means with which to assess whether the data may indicate a globally uniform signal such as might be characteristic of climatic warming. Given that most tide gauge sites are located in the Northern Hemisphere and are concentrated along the U.S. East Coast and around the Baltic Sea, such assessment is vital.

In the LR analysis, because of the highly inhomogeneous distribution of tide gauge sites, a simple site by site average of the secular RSL trends from the individual gauges could not be expected to provide a reasonable statistical estimate of the globally averaged trend. We have therefore divided the global ocean into seven distinct regions; the individual tide gauge estimates in each region were averaged and then weighted according to the fraction of the total surface area that each region represents to estimate the average rate of global sea level rise. These regions and their fractional areas are the northwestern Atlantic Ocean (8%), the southern Atlantic Ocean (15%), the Indian Ocean (20%), and the northwestern (12%), northeastern (10%), and south central (27%) Pacific Ocean.

In order to demonstrate the dominant sensitivities, the LR analyses were undertaken as a function of the minimum record length of the time series retained for analysis. For each choice of minimum record

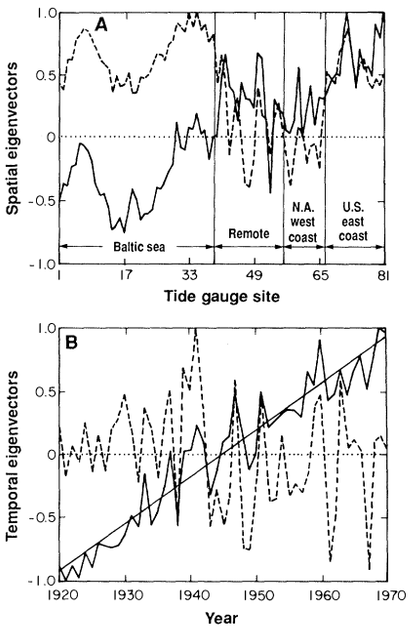

Fig. 6. Results for the global rate of sea level rise obtained from EOF analysis of the raw tide gauge data. Only the two dominant spatial (**A**) and temporal (**B**) eigenvectors (*13*) are shown. The dominant temporal eigenvector (solid line, B) determines the RSL rise signal that is common to the data (a linear least-squares fit to this eigenvector is superimposed); NA, North America.

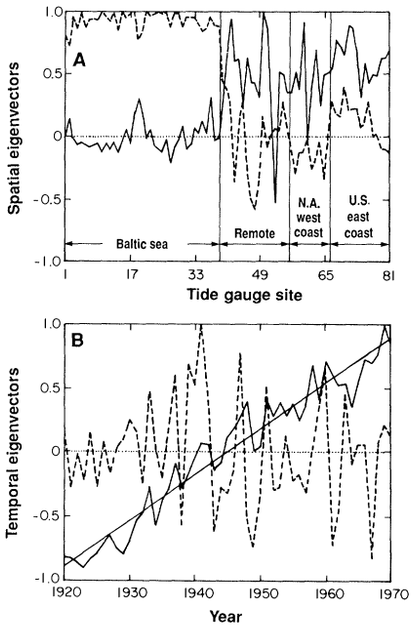

Fig. 7. Same as for Fig. 6 but for the reduced tide gauge data set constructed by subtracting the predicted isostatic signal from the raw RSL trend at each site.

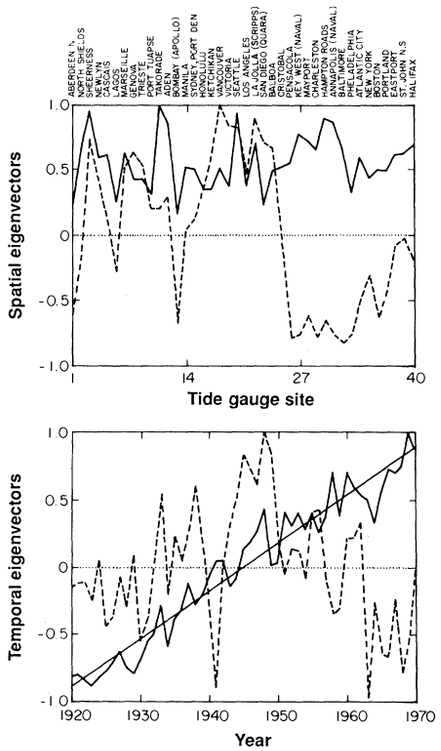

Fig. 8. Same as for Fig. 7 but for the reduced data from the 40 tide gauge stations with records of 50 years' duration that remain once the Baltic data are eliminated. Two additional records (Wajima, Japan, and Astoria, Oregon) have also been eliminated.

length, we computed a globally averaged rate of RSL rise using (i) an equal area average of the raw data, (ii) an equal area average of the reduced data generated by subtracting the isostatic adjustment component predicted with the geophysical model from the monthly mean tide gauge signals, and (iii) a direct site by site average of the reduced data (Fig. 5). As the minimum record length threshold increases, the number of tide gauges available for analysis drops sharply (dash-dotted line), and only 179 stations have records longer than 30 years' duration. Only 22 stations have records longer than 80 years and only 3 of these are located outside of the northeastern Atlantic sector; thus, the equal area average based on such long records is meaningless. From 30 to 80 years of minimum record length, the reduced site by site average (dotted line) steadily decreases from 1.3 to 0.9 mm per year whereas the reduced equal area average increases from 1.6 to 2.4 mm per year at 55 years and then decreases sharply to 1.2 mm per year. The equal area average of the raw data (dashed curve) mimics this variation but is lower by 0.4 to 0.5 mm per year. Correction of the tide gauge data for the influence of glacial isostatic adjustment therefore increases the inferred global rate of secular RSL rise irrespective of the minimum record length employed in the analysis. That this should be the case is clear from the form of the geophysical signal (Fig. 3).

The reason for the sharp fall of the estimate as the minimum record length increases beyond 60 to 70 years (see Fig. 5) is that almost all of the longest records are located in the Baltic Sea; because this is a region of rapid RSL fall due to ongoing postglacial rebound of the crust, the tide gauge records are swamped by this dominant signal, and smaller residual components cannot be measured accurately. We eventually delete Baltic Sea sites from the data set used to estimate the global RSL rise signal that could be associated with climatic warming. Estimates of the secular rate of RSL rise are reduced when the minimum record length is less than 30 to 40 years because the use of such short duration records precludes accurate estimation of the secular component of change. Between these two extremes, there is an approximate plateau in the estimated global rate between 40 and 50 years, and we suggest that this plateau represents a best trade-off between the number of records employed to make the estimate and the spatial coverage that these records provide. On this plateau, the equal area average of the reduced data suggests that the global rate of RSL rise is >2.0 mm per year.

The EOF method (*12, 13*) provides a means of assessing the spatial and temporal structures in the data and therefore whether the signal we have inferred through LR analysis is spatially coherent. Because EOF analysis is an "equal time" technique that requires that each tide gauge record be continuous and begin and end at the same dates, we restricted analysis to those records for which essentially continuous series are available from 1920 through 1970. We therefore chose records with lengths equal to that established with LR analysis as providing a best trade-off between length and spatial coverage. Any short gaps in the records (<10 years' duration) were filled with a linear least-squares interpolate, but the records with longer gaps were rejected. On this basis, 81 tide gauge records were selected. Earlier workers have performed EOF analyses on raw tide gauge data (*13*), but not on an isostatically reduced data set.

To demonstrate the impact that the isostatic adjustment correction has on the EOF estimate, we first present an analysis of the raw tide gauge data. The primary and secondary spatial and temporal eigenvectors (Fig. 6) account for 70% and 12%, respectively, of the total variance, and the form of the primary temporal eigenvector (solid line) demonstrates that there has been a consistent increase of sea level since 1920. The extent to which the primary spatial eigenvector (solid line) is spatially invariant indicates the extent to which the signal represented by the primary temporal eigenvector should be taken as global in scale.

Because this first spatial eigenvector is highly inhomogeneous, the EOF analysis on the raw data provides no support for the notion that there is a globally coherent signal that might be induced by climatic warming. However, the inhomogeneity in the spatial structure is strongly associated with the main centers of Pleistocene glaciation. For example, negative values of the first spatial eigenvector are almost exclusively associated with sites around the Baltic Sea. Large positive values are associated with sites along the East Coast of the United States, a region of rapid present-day postglacial submergence due to its location immediately peripheral to the Laurentide ice sheet. Moderately positive values obtain at sites located in regions remote from the main Pleistocene ice masses (the only exceptions are sites at Wajima, Japan, and Astoria, Oregon, which are both plausibly influenced by tectonic activity). Because the spatial heterogeneity in the first spatial eigenvector is basically the inverse of the geophysical signal due to glacial isostatic adjustment (Fig. 3), the heterogeneity should be substantially reduced once the tide gauge data are corrected for this contamination.

In the EOF analysis of the isostatically reduced tide gauge data set (Fig. 7), the magnitude of the first spatial eigenvector for all Baltic sites is near zero, indicating that the first temporal eigenvector has zero amplitude at these locations: as discussed above, crustal rebound completely masks any residual climatological signal in the RSL records at these locations. At the non–ice-covered sites, however, the magnitude of the first spatial eigenvector fluctuates about a well-defined mean value near 0.55, indicating that the linear RSL rise characteristic of the first temporal eigenvector is the main source of residual variance at all of these locations. This is clear evidence of the presence of a globally coherent signal.

If all of the Baltic sites at which the RSL signal is known to be swamped by crustal rebound are deleted, the resulting data set consists of 40 time series that we consider constitute the optimal data set for inference of the globally averaged rate of RSL rise. The primary eigenvalue from EOF analysis of this data set (Fig. 8) represents 67% of the variance and the secondary eigenvalue represents only 7%. The dominant spatial eigenvector (Fig. 8a, solid line) is now uniformly positive (Wajima and Astoria have been removed) with much reduced variations. The mean of 0.55 and small variations are indicative that the dominant temporal eigenvector (Fig. 8B, solid line) is characteristic of all sites in this data set and suggest that a rate of RSL rise near 2.4 ± 0.90 mm per year may be globally representative. Both EOF and LR estimates of the secular RSL trends at each of the final 40 tide gauge sites (Fig. 9) define a reasonably tight cluster.

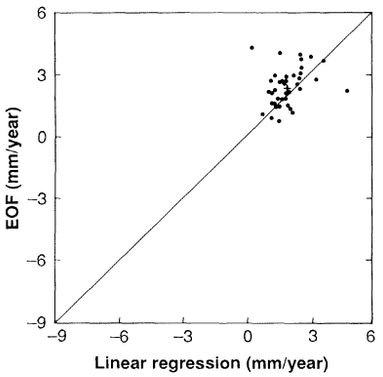

Fig. 9. Comparison between EOF and LR determination of the secular RSL trend at the 40 sites selected as the optimal set for the global inference. A reasonably tight cluster is delivered by the two types of analysis.

These analyses demonstrate that secular RSL trends recorded on tide gauge records of sufficient temporal duration are significantly contaminated by the ongoing process of glacial isostatic adjustment. Although the importance of this process in the geographical regions close to or coincident with those that were once ice-covered might be expected, our analyses have demonstrated that this signal is significant even at sites that are well removed from the centers of deglaciation. When this contamination is subtracted, then the residual rates of observed RSL rise reveal a signal that is nearly globally uniform, as might be characteristic of one caused by climatic warming. The remaining variability is easily understood as being a result of local tectonic activity. The rate of RSL rise (2.4 ± 0.90 mm per year) is strongly suggestive of the action of ongoing glacier and ice sheet melting. No more than 25% of this signal would appear to be explicable in terms of the steric effect of thermal expansion of the oceans (*1–3*).

Our analyses should not be construed as proof that global climate warming due to the enhanced greenhouse effect (or some other unknown cause) is occurring. The apparently required melting of high latitude continental ice could be caused by a long time scale but spatially localized internal climatic fluctuation. It would not be surprising, however, if the direct action of the expected enhancement of the greenhouse effect were first observed through an indirect response such as an increase in global sea level. The isostatically reduced RSL signal is an excellent integrator of global climatic change and we have shown that it is relatively immune from the extreme site-specific noise and locally induced secular variation (for example, the urban heat island effect) that is characteristic of measurements of the atmospheric temperature field.

REFERENCES AND NOTES

1. R. Etkins and E. S. Epstein, *Science* **215**, 287 (1982); A. Robock, *ibid.* **219**, 996 (1983); R. R. Revelle, in *Changing Climate* (National Academy of Sciences, Washington, DC, 1983), pp. 443–448.
2. V. Gornitz, S. Lebedeff, J. Hansen, *Science* **215**, 1611 (1982).
3. T. P. Barnett, *Clim. Change* **5**, 15 (1983); *J. Geophys. Res.* **89**, 7980 (1984).
4. M. F. Meier, *Science* **226**, 1418 (1984).
5. M. E. Schlesinger, *Adv. Geophys.* **26**, 141 (1984); K. Bryan, F. G. Komro, S. Manabe, M. J. Spelman, *Science* **215**, 56 (1982).
6. W. R. Peltier, *Adv. Geophys.* **24**, 1 (1982); *J. Geophys. Res.* **91**, 9099 (1986).
7. ———, *Rev. Geophys. Space Phys.* **12**, 649 (1974); *J. Geophys. Res.*, **90**, 9411 (1985); ——— and J. T. Andrews, *Geophys. J. R. Astron. Soc.* **46**, 605 (1976). P. Wu and W. R. Peltier, *ibid.* **70**, 435 (1982).
8. P. Wu and W. R. Peltier, *Geophys. J. R. Astron. Soc.* **74**, 377 (1983); *ibid.* **76**, 202 (1984); W. R. Peltier and P. Wu, *Geophys. Res. Lett.* **9**, 731 (1982); W. R. Peltier, *Nature* **304**, 434 (1983).
9. A. M. Tushingham and W. R. Peltier, in preparation.
10. W. R. Peltier, *Science* **240**, 895 (1988).
11. The tide gauge records were obtained from the archive of the Permanent Service for Mean Sea Level (PSMSL) at the Bidston Observatory, Birkenhead, Merseyside, England. From this data base, 554 records were individually verified by B. Braatz and D. Aubrey of the Woods Hole Oceanographic Institution. Our analyses are based on the 500 records in this subcollection that are of duration exceeding 10 years.
12. H. Hotelling, *J. Educ. Psychol.* **24**, 417 (1933); E. N. Lorentz, *Sci. Rep. 1* (Statistical Forecasting Project, Massachusetts Inst. of Technology, Cambridge, 1956).
13. In the EOF analysis of the tide gauge data set of RSL $M(x, t)$ where x is station location and t is time, we first removed the means of the individual series and reduced them to unit variance by computing $N(x, t) = [M(x, t) - \mu(x)]/\sigma(x)$, in which $\mu(x)$ is the individual mean height and $\sigma(x)$ the variance in the data of each station. The Orthogonal Function decomposition follows from the covariance matrices $\mathbf{A} = \mathbf{N}\,\mathbf{N}^T/n_x n_t$ and $\mathbf{B} = \mathbf{N}^T\,\mathbf{N}/n_x n_t$ where n_x and n_t are the numbers of spatial and temporal points in the data set, respectively. If we define spatial and temporal eigenvectors $\mathbf{E}$ and $\mathbf{C}$ such that $(\mathbf{A} - \lambda\mathbf{I})\,\mathbf{E} = 0$ and $(\mathbf{B} - \lambda\mathbf{I})\,\mathbf{C} = 0$ where $\mathbf{I}$ is the identity matrix and λ is a constant then we may decompose $\mathbf{N}$ as:

$$\mathbf{N}(x, t) = \sum_{k=1}^{n} \left[\lambda_k n_x n_t\right]^{1/2} \mathbf{E}_k(x)\ \mathbf{C}_k(t)$$

which is the orthogonal function representation on which the EOF analysis is based. By construction, the λ_k are the common eigenvalues of $\mathbf{A}$ and $\mathbf{B}$ while n is the smaller of n_x and n_t. The dominant eigenvalue provides a measure of the strength of the long-term rate of sea level rise and only it and the next smaller eigenvalue are explicitly analyzed. To estimate the local rate of RSL rise for the station at location x, we simply multiply the least-squares trend of $\mathbf{C}_1(t)$ by $(\lambda_1 n_x n_t)^{1/2}\,\mathbf{E}_1(x)$ and suppose that a global estimate is simply the site by site average of this product if the $\mathbf{E}_1(x)$ are uniform.
14. D. G. Aubrey and D. O. Emery, *Cont. Shelf Res.* **2**, 21 (1983). See also (*3*).

15. We are indebted to D. Aubrey and B. Braatz for providing the tide gauge data (*11*). T. Barnett provided useful commentary and R. Drummond provided computational assistance. This research was supported by research grant A9627 from the Natural Sciences and Engineering Research Council of Canada.

23 January 1989; accepted 11 April 1989